JOURNAL OF GEOPHYSICAL RESEARCH, VOL. 100, NO. C11, PAGES 22,667–22,679, NOVEMBER 15, 1995

A theoretical investigation of boundary layer flow and bottom shear stress for smooth, transitional, and rough flow under waves

Patricia L. Wiberg

Department of Environmental Sciences, University of Virginia, Charlottesville

Abstract. Velocity and shear stress distributions and the relationship between maximum near-bottom orbital velocity u_{om} and maximum shear velocity u_{*m} in an oscillatory boundary layer are computed for hydraulically smooth, transitional, and rough turbulent flow using unsteady boundary layer theory and a single, continuous expression for eddy viscosity K. Velocity profiles over a half wave cycle calculated using a time-independent form of K compare favorably with available measured profiles in smooth, transitional, and rough turbulent flows; computed shear stress profiles agree reasonably well with measured stress profiles. Use of a time-dependent eddy viscosity generally improves the agreement between measured and computed velocity and shear stress near the bed but not in the outer boundary layer. Maximum computed bottom shear stress, however, does not differ significantly from values calculated with a time-independent K owing to the choice of u_{*m} as the turbulent velocity scale in K. The ratio of maximum orbital velocity to maximum shear velocity is computed as a function of two nondimensional parameters, a Reynolds number $Re_*=u_{*m}\delta_w/\nu$ and an inverse Rossby number $\xi_0=\omega z_0/u_{*m}$; δ_w is wave boundary layer thickness, ω is wave frequency, ν is kinematic viscosity, and z_0 is the bottom roughness parameter. These independent variables of the nondimensional unsteady boundary layer equation can be related to the more commonly used wave boundary layer parameters which are expressed in terms of orbital velocity instead of shear velocity. At the fully rough and fully smooth turbulent flow limits, u_{*m}/u_{om} is given by a single curve as a function of ξ_0 or Re_*, respectively. These curves compare favorably with available measurements and expressions for wave friction factor. The nondimensional equations also yield the dependence of u_{*m}/u_{om} on ξ_0 and Re_* for transitionally rough turbulent flow.

Introduction

Near-bed wave velocities on the continental shelf are often comparable in magnitude to near-bed current velocities (including wind-driven currents and tides) during low to moderate wave conditions and can become considerably larger on the mid- and inner shelf, particularly during periods of large swell. Comparable wave and current velocities near the bed translate into boundary shear stress values for the wave component of flow that are considerably larger than those associated with the current owing to differences in wave and current boundary layer scales. High wave-generated shear stresses readily mobilize the finer fractions of typical continental shelf bed sediments and deform beds of predominantly sand-sized sediment into symmetrically shaped ripple forms. Initial motion of sediment, bedload transport, ripple geometry, and ripple migration rates are wave-dominated processes over much of the continental shelf. In addition, shear stress, bottom roughness, velocity profile structure, and suspended sediment distribution in the bottom boundary (Ekman) layer are significantly influenced by the dynamics of the wave boundary layer.

Paper number 95JC02377.
0148-0227/95/95JC-02377$05.00

Despite the importance of wave boundary layer dynamics to near-bed flow and sediment transport, direct field measurements of flow in the wave boundary layer on the continental shelf are almost nonexistent because of the technical difficulties of making velocity measurements within 10 cm of the bed, which is typically irregular, in water tens of meters deep. As a result, it has been necessary to rely on oscillatory boundary layer models to provide estimates of velocity and shear stress in the wave boundary layer and of wave boundary layer height for near-bed velocity and sediment transport calculations on the continental shelf. Recent developments in laser velocimetry, such as the instrument described by *Agrawal and Aubrey* [1992], may soon provide direct measurements of wave boundary layer velocity on the continental shelf. Such measurements will be valuable for testing the models, but it is unlikely that they will become routine in the near future. Our reliance on wave boundary layer models for predictions of flow and sediment transport on the shelf and for interpreting near-bed measurements makes it important that these models be as complete and as accurate as possible.

Our understanding of wave boundary layer dynamics is based on 30 years of experimental flume and wind tunnel studies [e.g., *Jonsson*, 1963; *Kamphuis*, 1975; *Jonsson and Carlsen*, 1976; *Hino et al.*, 1983; *Sleath*, 1987; *Jensen et al.*, 1989] and theoretical analyses [e.g., *Kajiura*, 1968; *Smith*, 1977; *Grant and Madsen*, 1979; *Long*, 1981; *Brevik*, 1981;

Myrhaug, 1982; *Trowbridge and Madsen*, 1984; *Fredsøe*, 1984]. Much of this work focuses on velocity structure and shear stress in hydraulically rough oscillatory boundary layers. One of the motivations for these studies has been to establish the relationship between maximum near-bed wave orbital velocity u_{om} and maximum wave-generated boundary shear stress τ_{0m} or maximum shear velocity u_{*m} as is necessary for calculations of sediment transport and wave energy dissipation under surface gravity waves. The most widely used relationship between orbital velocity and boundary shear stress is the semiempirical wave friction factor diagram developed by *Jonsson* [1966] who expresses friction factor f_w as a function of the ratio of near-bed wave orbital amplitude to physical bottom roughness length a_o/k_s and a wave Reynolds number $Re_o=u_{om}a_o/\nu$; ν is kinematic viscosity.

The traditional focus on rough turbulent wave boundary layers stems from its prevalence in natural settings and the relative simplification achieved by being able to disregard the viscous sublayer. It is often argued that oscillatory flows in the coastal environment are generally hydraulically rough. Hydraulically smooth and transitional turbulent flows can exist, however, particularly in lower-energy environments or in the absence of oscillatory ripples which greatly increase bed roughness. A few studies have attempted to characterize a broader range of flow conditions. *Jonsson's* [1966] wave friction factor diagram extends through rough, transitionally rough, and smooth turbulent flow and laminar flow based on a combination of theoretical and semiempirical expressions for these flow regimes. The theoretical studies of *Kajiura* [1968] and *Fredsøe* [1984] include viscous sublayer effects in order to compute velocity distributions for smooth and transitionally rough turbulent flows. *Hino et al.* [1983] measured velocity and turbulence profiles in a smooth, transitionally turbulent, oscillating wind tunnel flow. More recently, *Jensen et al.* [1989] carried out an extensive set of flume experiments of velocity and turbulence structure in smooth, transitionally rough, and rough turbulent oscillatory boundary layers.

In this paper a theoretical formulation for velocity and shear stress in wave boundary layers under conditions ranging from smooth to rough turbulent flow is presented in order to address three issues relevant to the use of wave boundary layer models in continental shelf environments. The first is whether a single expression for eddy viscosity can be used to characterize profiles of velocity and shear stress in turbulent oscillatory boundary layers for all hydraulic roughness conditions, i.e., all roughness Reynolds numbers. The eddy viscosity formulation proposed herein is similar in nature to the form used by *Kajiura* [1968] but is smooth and continuous in the vertical. The data of *Jensen et al.* [1989] provide excellent tests for these calculations. Also considered here is whether a time-independent eddy viscosity, such as is used in most oscillatory boundary layer models, provides sufficiently accurate profiles of velocity and shear stress over a full wave cycle. To address this question, velocity and shear stress computed using a time-independent eddy viscosity are compared with results using a time-varying form similar to that proposed by *Trowbridge and Madsen* [1984]. Finally, the model is used to generate curves characterizing the ratio of maximum bottom shear velocity to maximum bottom orbital velocity for the full range of turbulent flow conditions. The limiting curves for rough turbulent flow and smooth turbulent flow are compared to existing expressions and data for the wave friction factor.

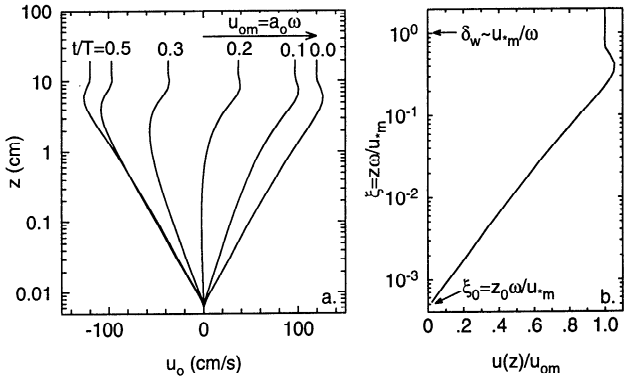

Figure 1. (a) Example of velocity profiles in an oscillatory rough turbulent boundary layer over a half wave period. (b) Profile of velocity at maximum flow conditions ($u_o=u_{om}$), normalized by maximum orbital velocity u_{om} as a function of nondimensional height above the bed $\xi=z/\delta_w=z\omega/u_{*m}$. In this example, u_{om}=120 cm/s, T=12 s, u_{*m}=7.8 cm/s, and z_0=0.007 cm.

Unsteady Boundary Layer Equations

When water depth h is less than about half the wavelength L of a surface gravity wave, wave orbital motion will be present at the bed. For waves of small steepness, parameters such as wave orbital velocity and orbital diameter can be calculated using small-amplitude wave theory. The wide applicability of small-amplitude wave theory outside of the nearshore zone makes it relatively straightforward to estimate inviscid wave velocity at the bed, given estimates of wave height, period, and water depth [e.g., *Madsen*, 1976]. This theory assumes that the bed is frictionless, but owing to the no-slip condition at the bed surface, a thin wave boundary layer exists at the bed in which the velocity increases from zero to the near-bed orbital velocity u_o (Figure 1). As near-bed orbital velocity varies through a wave period, so does the velocity structure in the wave boundary layer and the shear stress at the bed. A phase difference ϕ exists between maximum orbital velocity at the top of the boundary layer u_{om} and maximum boundary shear stress τ_{0m} which depends on the velocity gradient at the bed.

Velocity Distribution in an Oscillatory Boundary Layer

The velocity structure in the wave boundary layer and the relationship between boundary shear stress τ_0 or shear velocity $u_*=(\tau_0/\rho)^{1/2}$ and near-bed orbital velocity can be computed using the turbulent boundary layer momentum equation for an unsteady flow; ρ is fluid density. The unsteady boundary layer approximation to the Reynolds-averaged horizontal momentum equation with an eddy viscosity closure has the form

$$\frac{\partial u}{\partial t}=-\frac{1}{\rho}\frac{\partial p}{\partial x}+\frac{\partial}{\partial z}K(z)\frac{\partial u}{\partial z} \qquad (1)$$

where u is horizontal velocity in the wave boundary layer, p is pressure, and $K(z)$ is eddy viscosity. This can be coupled

to an inviscid flow approximation for the velocity above the boundary layer,

$$\frac{\partial u_o}{\partial t}=-\frac{1}{\rho}\frac{\partial p}{\partial x} \tag{2}$$

to produce

$$\frac{\partial u}{\partial t}=\frac{\partial u_o}{\partial t}+\frac{\partial}{\partial z}K(z)\frac{\partial u}{\partial z} \tag{3}$$

Alternatively, (3) can be written in terms of velocity differences as

$$\frac{\partial}{\partial t}(u_o-u)=\frac{\partial}{\partial z}K(z)\frac{\partial}{\partial z}(u_o-u) \tag{4}$$

using the fact that $\partial u_o/\partial z\approx 0$ in the wave boundary layer.

If the wave motion is assumed to be sinusoidal, then the time dependence of the velocity field can be made explicit by writing $u_o-u=\mathrm{Re}(Ue^{i\omega t})$, where $\omega=2\pi/T$ and T is wave period [e.g., *Smith*, 1977]. In this case, (4) can be written as an ordinary differential equation in terms of the complex velocity U,

$$\frac{d^2U}{dz^2}+\frac{dK/dz}{K}\frac{dU}{dz}-\frac{i\omega}{K}U=0 \tag{5}$$

The boundary conditions are (1) $U=u_o$ at $z=z_0$ and (2) $U=0$ for $z\gg\delta_w$; z_0 is the hydrodynamic roughness parameter and δ_w is wave boundary layer height. An expression for the eddy viscosity $K(z)$ must be specified before (5) can be solved. If eddy viscosity is linear in z, e.g., $K=\kappa u_{*m}z$, where κ is von Karman's constant or if it is linear near the bed and constant in the outer boundary layer, then (5) can be solved analytically [e.g., *Kajiura*, 1968; *Smith*, 1977; *Grant and Madsen*, 1979; *Brevik*, 1981; *Myrhaug*, 1982]. These analytical solutions show that the velocity profile approaches a logarithmic form in the limit as z gets small and they can be differentiated to obtain explicit expressions for shear velocity. Equation (5) can also be solved numerically using Thomas' tridiagonal algorithm [e.g., *Carnahan et al.*, 1969] for an arbitrary choice of eddy viscosity.

Eddy Viscosity

Several choices for eddy viscosity are possible. *Jonsson* [1963, 1966], *Smith* [1977], and *Grant and Madsen* [1979] used the linear form $K(z)=\kappa u_{*m}z$ because it allowed an analytical solution and because it was expected to have the proper form near the bed. It also has been shown to yield velocity profiles in reasonable agreement with velocity measurements made by *Jonsson* [1963; *Jonsson and Carlsen*, 1976] in a rough turbulent oscillatory flow. On the other hand, a linearly increasing K is not physically reasonable near the top of the wave boundary layer, where the shear stress goes to zero in the absence of a superimposed current, or to the current stress if a current exists. *Long* [1981], following work on atmospheric boundary layers by *Businger and Arya* [1974], proposed the alternative form $K(z)=\kappa u_{*m}ze^{-z/l}$, where l is a length scale. This expression for eddy viscosity approaches the linear form for small values of z, reaches a maximum at $z=l$, and then decays with height for $z>l$. Long proposed that l for high-frequency, oscillating flows should have the form $l=u_{*m}/6\omega$. Wave velocity profiles calculated using this eddy viscosity also agree well with *Jonsson's* [1963] measurements of oscillatory velocity [*Long*, 1981]. *Kajiura* [1968], *Brevik* [1981], and *Myrhaug* [1982] used segmented eddy viscosity profiles, typically of the form $K=\kappa u_{*m}z$ for $z<z^*$ and $K=\kappa u_{*m}z^*$ for $z\geq z^*$, where z^* is a matching height within the wave boundary layer. *Kajiura* [1968] also included a third segment to characterize the viscous sublayer for smooth and transitionally rough turbulent flows, taking $K=\nu$ for $z<\delta_\nu$, where δ_ν is viscous sublayer height.

All of these expressions for eddy viscosity are time-independent, with the turbulent velocity scale represented by maximum shear velocity. Use of a time-independent eddy viscosity for high-frequency, oscillatory flow is justified by *Long* [1981], provided that the timescale for decay of the turbulent eddies is long relative to the period of oscillation for the waves. *Long* [1981] obtained good agreement between velocity profiles calculated using a time-independent eddy viscosity and those measured by *Jonsson* [1963], both at times of maximum and near-zero orbital velocity (see Figure 2).

Trowbridge and Madsen [1984] gave further consideration to the question of a time-independent versus time-dependent form of eddy viscosity for turbulent wave boundary layers. They proposed a relatively simple, time-dependent expression for eddy viscosity that yields a velocity profile when $u_o=u_{om}$ (maximum velocity) for the first harmonic of velocity that compares well with the

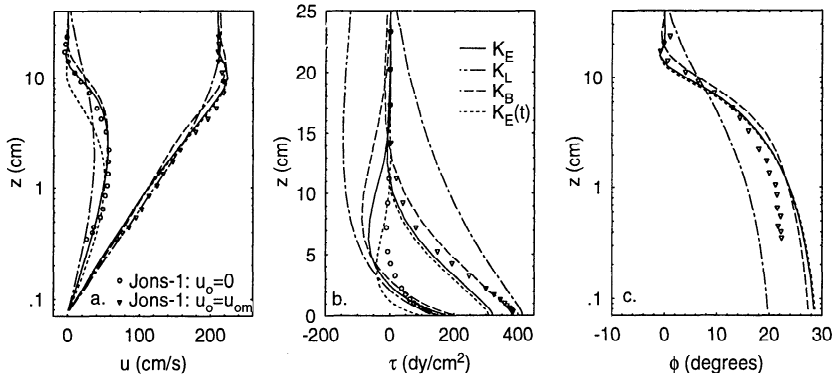

Figure 2. Comparison of computed profiles of wave velocity, shear stress, and phase for rough turbulent flow and *Jonsson*'s [1963; *Jonsson and Carlsen*, 1976] measured profiles for $\omega=0.75\ \mathrm{s}^{-1}$, $u_{om}=210$ cm/s, and $z_0=0.077$ cm. Computed profiles are shown for the following three choices of eddy viscosity: $K_E=\kappa u_{*}ze^{-z/l}$; $K_L=\kappa u_{*}z$; $K_B=\kappa u_{*}z$ for $z\leq z^*$ and $K_B=\kappa u_{*}z^*$ for $z>z^*$, where $z^*=\kappa u_{*}/6\omega$. (a) Velocity profiles at $u_o=0$ and $u_o=u_{om}$. (b) Shear stress at $u_o=0$ and $u_o=u_{om}$. (c) Phase difference between $u(z)$ and u_{om} at maximum velocity.

corresponding profile measured by *Jonsson* [1963; *Jonsson and Carlsen*, 1976, test I]. In addition, their expression for the third harmonic of velocity also provides reasonable agreement with the third harmonic of the *Jonsson* [1963; *Jonsson and Carlsen*, 1976, test 1] measurements. This term cannot be computed with a time-independent form of eddy viscosity [*Trowbridge and Madsen*, 1984]. While *Trowbridge and Madsen* [1984] were able to calculate higher harmonics of the velocity field in a wave boundary layer, they also note that the magnitude of the third harmonic of velocity is only a few percent of the fundamental harmonic, and the third harmonic of shear stress is 20-25% of the first harmonic for small-amplitude waves [*Trowbridge and Madsen*, 1984]. Given the number of sources of uncertainty in estimates of boundary shear stress of the same order, it is reasonable to begin with a time-independent formulation.

To examine smooth and transitionally rough turbulent oscillatory flows, a characterization of the viscous sublayer must be included in the profiles through use of an appropriate form of eddy viscosity close to the bed. *Kajiura* [1968] let $K=\nu$ for $z<\delta_\nu$ for smooth turbulent flow. *Reichardt* [1951] and *van Driest* [1956] derive expressions for the velocity profile of a smooth turbulent unidirectional flow that extend through both the viscous sublayer and the overlying turbulent logarithmic layer, with smooth transitions between the two regions [see *Schlichting*, 1979]. *Van Driest* [1956] divides the shear stress into a viscous stress and a Reynolds stress and defines a modified mixing length for the Reynolds stress, $L=\kappa z^+[1-\exp(-z^+/26)]$ that goes to zero at small values of $z^+=u_* z/\nu$ and to κz at large values of z^+. An additional term of $\exp(-60z^+/26R_*)$ is added to L for the case of transitionally rough turbulent flow. *Reichardt* [1951] formulates the problem in terms of the ratio of Reynolds stress to viscous stress, which is then used to obtain an expression for velocity, $u/u_*=\kappa^{-1}(1+\kappa z^+) + c[1-\exp(-z^+/11) - (z^+/11)\exp(-0.33z^+)]$, that approaches z^+ as z goes to zero and $\kappa^{-1}\ln(z^+/z_0^+)$ for $z^+>\delta_\nu$; $c=-\kappa^{-1}[\ln(z_0^+)+\ln\kappa]$. *Reichardt* [1951] developed this expression for smooth turbulent flow, in which case $z_0^+=0.11$ and $c=7.8$. However, his equation can also be considered to provide an interpolation of the velocity structure for the transition layer between the viscous sublayer and the overlying region of fully turbulent flow, much in the same way as van Dreist's, by appropriate choice of z_0^+. Comparison of van Dreist's formulation, including the term for transitionally rough flow, and Reichardt's expression over roughness Reynolds numbers $R_*=u_* k_s/\nu$ ranging from 1 to 1000 indicates that the two formulations yield nearly indistinguishable velocity profiles over that range.

An objective of this investigation was to incorporate one of these expressions into the eddy viscosity formulation to provide a single eddy viscosity profile that will yield a velocity profile that varies smoothly through the full wave boundary layer. Either of the *Reichardt* [1951] and *van Driest* [1956] formulations can be expressed as an eddy viscosity. I chose to use the *Reichardt* [1951] formulation because I have used it previously to represent near-bed velocity structure for transitionally rough turbulent flow [*Wiberg and Smith*, 1987] with good results and it can be readily incorporated into a general formulation for eddy viscosity, giving

$$\frac{1}{K}=\frac{1}{\nu}\left\{\frac{1}{1+\kappa z^+ f(z/l)}+\frac{c}{11.6}\left[e^{-z^+/11.6}+(0.33z^+-1)e^{-0.33z^+}\right]\right\} \quad (6)$$

where $c=-\kappa^{-1}[\ln(z_0^+)+\ln\kappa]$; $f(z/l)=1$ for the linear eddy viscosity, $f(z/l)=l/z$ for $K=\kappa u_* l$, and $f(z/l)=e^{-z/l}$ for the exponential form. At large values of z^+ the eddy viscosity given by (6) approaches $\kappa u_* z f(z/l)$, while at small values of z^+ it approaches ν, as expected.

Equations (5) and (6) can be used to generate velocity and shear stress profiles for smooth, transitionally rough, or rough turbulent oscillatory flows, given period, bottom roughness length, and either maximum shear velocity u_{*m} or maximum bottom orbital velocity u_{om}; if u_{om} is given, the solution is obtained iteratively. The roughness parameter z_0 is determined from a fit to *Nikuradse*'s [1932, 1933] measurements of z_0/k_s as a function of R_* [*Smith*, 1977] (original data are given by *Schlichting* [1979, p. 620]).

Nondimensionalization of the Wave Boundary Layer Equations

Solutions to (5) can be obtained in a more general form if the equations are nondimensionalized. The appropriate nondimensionalization is suggested by Figure 1b, in which only the profile corresponding to the maximum near-bed orbital velocity u_{om} is shown. If the velocity $u(z)$ is normalized by u_{om}, then the slope of the velocity profile in the wave boundary layer depends on the ratio of z_0 to δ_w. Assuming $\delta_w=u_{*m}/\omega$ to within a constant factor of order 1, $z_0/\delta_w=\omega z_0/u_{*m}$. This suggests using the nondimensional vertical coordinate,

$$\xi=z\omega/u_{*m}, \quad (7)$$

which has the form of an inverse Rossby number. Transforming (5) into these nondimensional variables gives

$$\frac{d^2U^*}{d\xi^2}+\frac{dK/d\xi}{K}\frac{dU^*}{d\xi}-\frac{iu_{*m}^2}{\omega K}U^* = \frac{d^2U^*}{d\xi^2}+\frac{dK^*/d\xi}{K^*}\frac{dU^*}{d\xi}-\frac{iU^*}{K^*}=0 \quad (8)$$

where $U^*=U/u_{om}$ and K^* is nondimensional eddy viscosity $K\omega/u_{*m}^2$. *Reichardt*'s [1951] expression for eddy viscosity (6) nondimensionalized in this way is

$$\frac{1}{K^*}=Re_*\left\{\frac{1}{1+\kappa Re_*\xi f(\xi)}+\frac{c}{11.6}\left[e^{-\xi Re_*/11.6}+(0.33\xi Re_*-1)e^{-0.33\xi Re_*}\right]\right\} \quad (9)$$

where

$$Re_*=\frac{u_{*m}^2}{\omega\nu} \quad (10)$$

and the z^+ terms in (6) have been replaced by the equivalent ξRe_*; $f(\xi)=1$ for the linear eddy viscosity and $f(\xi)=e^{-6\xi}$ for the exponential form of K. K^* as given by (9) is a function of ξ and Re_*. At large values of Re_*, K^* approaches $\kappa\xi f(\xi)$, while at small values of Re_*, K^* approaches Re_*^{-1}. The upper boundary condition for (8) is $U^*=0$ for $\xi\gg 1$. The boundary condition at the bottom is $U^*=1$ at $\xi=0$ for smooth and transitionally rough turbulent flow; this condition is applied at $\xi=\xi_0=z_0\omega/u_*$ for rough turbulent flow. When solving these equations, the lower boundary condition is evaluated at $\xi=0$ when the value of $c=-\kappa^{-1}[\ln\xi_0 Re_*+\ln\kappa]$ in

(9) is greater than -1 and at $\xi=\xi_0$ when c<-1; c=-1 at a roughness Reynolds number $R_*=u_*k_s/\nu=z^+k_s/z_0\approx 110$.

Under rough turbulent flow conditions ($R_* > 70-100$) the viscous sublayer is negligibly thin relative to the size of the physical roughness elements, K^* becomes independent of Re_*, and the solution to (8) requires only that ξ_0 be specified. In this case the ratio of the bed roughness parameter to physical bed roughness length z_0/k_s is a constant approximately equal to 1/30 [*Nikuradse*, 1933], so the product $\xi_0 Re_* = z_0^+ = R_* z_0/k_s$ takes the value $R_*/30$. This places a lower limit on Re_* for rough flow at a given ξ_0 of $Re_* \approx 3/\xi_0$, assuming fully rough conditions for $R_*>100$. In contrast, smooth flow occurs when $R_*<3-5$. In this limit, $z_0=\nu/9u_*$ or $z_0/k_s = (9R_*)^{-1}$ [*Nikuradse*, 1932], giving $Re_*\xi_0 = R_* z_0/k_s=0.11$ or $\xi_0 \approx (9Re_*)^{-1}$. Thus the solution depends only on Re_* for smooth turbulent flow. For transitional conditions the flow depends on both Re_* and ξ_0. These asymptotic dependencies are analogous to the results of Kajiura [1968] and Jonsson [1966], showing that the single independent parameter for smooth flows is Re_o and for rough flows is a_o/k_s.

The existence of a meaningful solution to (8) places some additional constraints on the range of possible values of the independent parameters ξ_0 and Re_*. For example, there must be adequate separation in value between z_0 and δ_w (see Figure 1). As this ratio approaches 1, the solution breaks down. Velocity profile structure and the relationship between u_{*m}/u_{om} and ξ_0 ($\sim z_0/\delta_w$) support a maximum value of ξ_0 of roughly 0.03. This implies that for fully rough flows δ_w must be comparable to or greater than k_s. The upper limit $\xi_0=0.03$ can be related to a criterion in terms of a_o/k_s. For rough flow, $a_o/k_s = u_{om}/(\omega 30 z_0) = (30\xi_0 u_{*m}/u_{om})^{-1}$. The computed value of u_{*m}/u_{om} for $\xi_0=0.03$ is 0.14 (wave friction factor $f_w=0.04$), which corresponds to $a_o/k_s=8$. A value of $a_o/k_s=10$ has been cited as a lower limit of a_o/k_s for theoretical rough-flow friction factors which are based on a linear eddy viscosity near the bed [*Jonsson*, 1963], so the two limits are consistent. A further constraint occurs at small values of wave Reynolds number because of the laminar-turbulent flow transition. This transition occurs at $Re_o \approx 10^5-10^6$ [*Jensen et al.*, 1989; Figure 8] or Re_* of the order of 1000. This provides an approximate lower limit on the wave Reynolds number for turbulent oscillatory boundary layer flow.

Comparison of Measured and Computed Profiles of Velocity and Shear Stress

The most widely cited oscillatory flow measurements are those made in a rough oscillatory boundary layer by *Jonsson* [1963; *Jonsson and Carlson*, 1976]. The relevant flow parameters for this case are u_{om}=210 cm/s, ω=0.75 s^{-1}, and k_s=2.3 cm (case Jons 1; see Table 1). Measured velocity profiles for $u_o=0$ and $u_o=u_{om}$ are indicated by the symbols in Figure 2a; the profile shown for $u_o=u_{om}$ is an average of the measured velocity profiles at $u_o=\pm u_{om}$. The curves represent profiles calculated using (5) and (6) at the same phases for three different forms of time-independent eddy viscosity (identified in the legend): $K_E=\kappa u_{*m} z e^{-z/l}$; $K_L=\kappa u_{*m} z$; and $K_B=\kappa u_{*m} z$ for $z\le z^*$, $K_B=\kappa u_{*m} z^*$ for $z>z^*$, where $z^*=\kappa l=\kappa u_*/(6\omega)$, following *Trowbridge and Madsen* [1984]; a time-dependent form of K_E is also plotted in Figure 2 and is discussed in the next section. Of the time-independent forms of eddy viscosity the exponential (K_E) and the two-part (K_B) forms of K provide the closest agree-

Table 1. Oscillatory Boundary Layer Measurements

Case *	T s	u_{om}, cm/s	u_{*m}, cm/s	k_s, cm	ξ_0 $\times 10^{-4}$	Re_*† $\times 10^3$	Re_o $\times 10^5$	(u_{*m}/u_{om}), Measured	Flow ‡	(u_{*m}/u_{om}), Model§
Jens 1	9.72	7.3	0.77		14.	0.081	0.075	0.106	L	0.110
Jens 2	9.72	15.2	1.1		6.8	0.16	0.33	0.072	L	0.081
Jens 3	9.72	23.0	1.4		4.2	0.13	0.75	0.061	L	0.067
Jens 4	9.72	34.0	1.7		2.8	0.39	1.6	0.050	L	0.062
Jens 5	9.72	45.0	2.3		1.6	0.72	2.9	0.051	L/S	0.057
Jens 6	9.72	60.0	3.2		0.80	1.4	5.0	0.053	L/S	0.053
Jens 7	9.72	68.0	3.5		0.67	1.7	6.5	0.052	L/S	0.052
Jens 8	9.72	102.0	4.8		0.36	3.1	16.	0.047	S	0.048
Jens 9	9.72	155.0	6.4		0.20	5.6	34.	0.041	S	0.044
Jens 10	9.72	200.0	7.7		0.14	8.1	60.	0.039	S	0.042
Jens 12	9.72	102.0	5.8	0.084	3.1	4.57	16.	0.057	T	0.061
Jens 13	9.72	200.0	11.	0.084	1.7	16.4	60.	0.055	T/R	0.057
Jens 14	8.12	87.0	6.0	0.260	11.	4.1	9.0	0.069	R	0.075
Jens 15	8.12	210.0	14.	0.370	6.8	22.	52.	0.067	R	0.069
Jons 1	8.39	210.0	21.	2.3	25.	52.	53.	0.095	R	0.090

Abbreviations are defined as follows: T, wave period; u_{om}, maximum near-bottom orbital velocity; u_{*m}, maximum shear velocity; k_s, physical bottom roughness length; ξ_0, nondimensional bottom roughness parameter; Re_*, Reynolds number; Re_o, wave Reynolds number.

* Jens is *Jensen et al.* [1989]; Jons is *Jonsson* [1963]. Numbers indicate experiment number.

† Viscosity is 0.0114 cm^2/s for the *Jensen et al.* [1989] cases and 0.010 cm^2/s for the *Jonsson* [1963] experiment (based on values provided by *Jonsson and Carlson* [1976]).

‡ L is laminar flow, S is smooth turbulent flow, R is rough turbulent flow, and L/S is laminar-smooth transitionally turbulent flow.

§ Model calculations use equations (5) and (6) with the exponential form of eddy viscosity K_E.

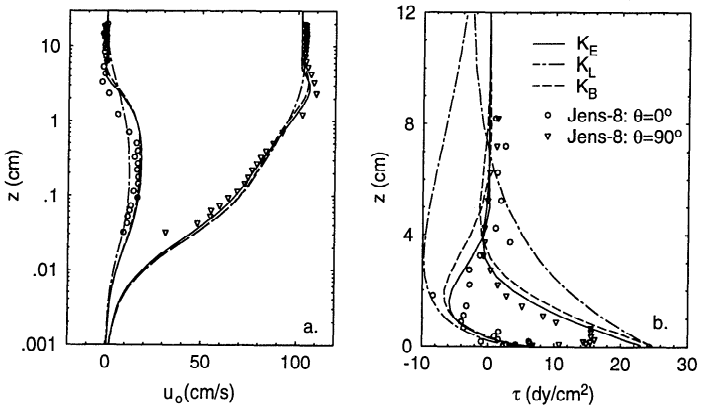

Figure 3. Comparison of computed profiles of wave velocity and shear stress for smooth turbulent flow with the *Jensen et al.* [1989] measured profiles for case Jens 8 in Table 1 at u_o=0 and u_o=u_{om}; T=9.7 s, u_{om}=102 cm/s.

ment with measured velocity; K_E results in modestly better agreement than K_B.

Shear stress profiles estimated by *Jonsson and Carlson* [1976, test 1] from the velocity data using the momentum integral method are compared to calculated stress profiles in Figure 2b. The exponential and two-part forms of eddy viscosity provide the best agreement between measurement-derived and computed profiles of shear stress, although none of the calculated profiles closely follows the measurements between z=2 and 14 cm for u_o=0. Maximum shear velocity was best estimated by the linear and two-part forms of K (K_L and K_B). Measured and calculated phase difference ϕ between u_{om} and velocity at each level when u_o=u_{om} is shown in Figure 2c. Again, K_E and K_B provide the best agreement, but both deviate from the measurements near the bed.

Jensen et al. [1989; *Jensen*, 1989] measured velocity and shear stress in laminar, transitionally turbulent, and smooth, transitionally rough, and rough turbulent oscillatory boundary layers. These measurements were made in a water tunnel using a laser-Doppler anemometer (LDA) and hot film probe for a range of Reynolds numbers [*Jensen et al.*, 1989]; flow parameters for these measurements are listed in Table 1. Tabulated profiles of mean velocity, Reynolds stress, and turbulence intensity measured at 15° phase increments over a half wave cycle are available for cases Jens 8, 10, 12, and 13 (Table 1) in the work of Jensen [1989]. Time series of mean and rms values of bottom shear stress, measured directly by hot film, were also provided (J. Fredsøe, personal communication, 1992) for the laminar (Jens 1-5, Table 1) and smooth turbulent (Jens 7-10, Table 1) cases.

Measured velocity and shear stress profiles for a smooth turbulent flow (Re_o=1.6×10^6) with T=9.72 s and u_o=102 cm/s (case Jens 8, Table 1) are shown by the symbols in Figures 3a and 3b, respectively, for u_o=0 (θ=0) and u_o=u_{om} (θ=90°; profiles at 30° phase increments are shown in Figure 5). The curves are the velocity profiles calculated from (5) and (6) for the same wave conditions. The agreement between the measured and predicted velocity profiles is good for the exponential K_E and two-part K_B forms of eddy viscosity, except near the top of the boundary layer when u_o=0. The overestimate of velocity in this case may be a result of using a time-independent eddy viscosity and the laminar flow conditions present near the bed at this phase (see discussion below). Channel-flow measurements of velocity profiles in smooth turbulent flows indicate that the top of the transition zone between the viscous sublayer and the region of logarithmically varying velocity occurs at a distance of roughly z^+=30 [*Schlichting*, 1979; *Nezu and Rodi*, 1986]. This corresponds to z≈0.07 cm for the case shown in Figure 3 (Jens 8, Table 1) and appears to provide a reasonable estimate of the lower extent of the region of logarithmically varying flow.

The exponential and two-part eddy viscosities also yield reasonably good agreement between computed shear stress and measured Reynolds stress (Figure 3b); computed values represent the sum of the Reynolds and viscous stresses and thus deviate from the measured stresses close to the bottom. As in the rough flow case (Figure 2b), the linear eddy viscosity K_L gives nonzero values of shear stress much higher into the boundary layer than are indicated by the data. Maximum boundary shear stress for this case was closely estimated by the model using K_E (Table 1).

The *Jensen et al.* [1989] data also provide measured profiles of velocity and shear stress for a case of transitionally rough turbulent flow with the same period and maximum orbital velocity as Jens 8 (Figure 3) but with a larger bottom roughness parameter (Jens 12, Table 1). For the transitionally rough flow measurements the bottom of the water tunnel was covered with sand paper having a mean grain size of 0.035 cm. *Jensen et al.* [1989] estimate the physical roughness length k_s for this case to be 0.084 cm based on measured velocity profiles. The roughness Reynolds number R_* computed from the measurements is 43, well within the range of transitionally rough turbulent flow conditions. The measured and calculated velocity and shear stress profiles are shown in Figures 4a and 4b. The agreement is similar to that shown in Figure 3 for a smooth flow, except that the measured and computed values are closer at u_o=0 with a time-independent K for this transitionally rough flow; both velocity and shear stress profiles computed using K_E closely track the measurements.

Hino et al. [1983] measured velocity and turbulence structure in a smooth, transitionally turbulent oscillatory wind tunnel flow. The flow conditions for their measurements were T=3.18 s and Re=$\hat{U}d/\nu$=2.25×10^4, where $\hat{U}$ is the amplitude of the cross-sectional mean velocity variation; wind tunnel height d=10 cm, and ν=0.15 cm^2/s. Plots of measured profiles of *Hino et al.* [1983] indicate that u_{om}≈

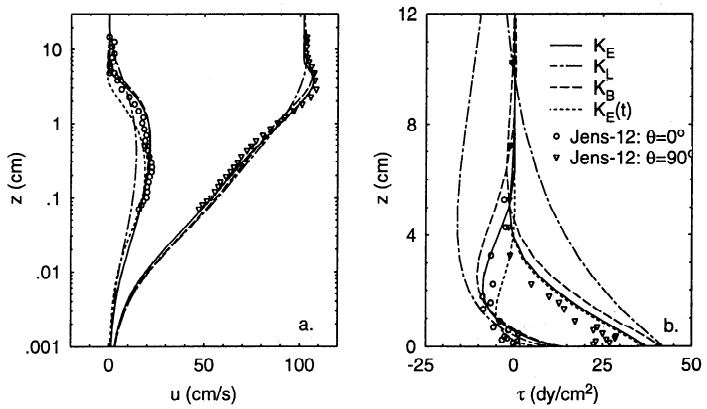

Figure 4. Comparison of profiles of wave velocity and shear stress measured by *Jensen et al.* [1989] for a case of transitionally rough turbulent flow (Jens 12, Table 1) with profiles computed using (5); T=9.7 s, u_{om}=102 cm/s.

300 cm/s, giving $Re_o=u_{om}^2/(\omega\nu)\approx 3.0\times10^5$, within the laminar to turbulent transition range indicated by the *Jensen et al.* [1989] data (see Figure 8). The *Hino et al.* [1983] measurements of Reynolds stress and estimates of turbulence production indicate that the boundary layer is laminar at the beginning of the accelerating phase. The onset of turbulence occurs rapidly near the end of the accelerating phase and decreases gradually in the second half of the decelerating stage. Similar variations of wall shear stress with phase were observed by *Jensen et al.* [1989] for a case in which $Re_o=2.9\times10^5$ (Jens 5, Table 1); the data indicate that the onset of turbulence in this case was delayed until the beginning of the decelerating phase. The present model assumes fully turbulent flow and cannot represent the velocity structure during the onset of turbulence in an oscillatory boundary layer. Thus use of the model to compute the velocity field through a wave cycle is restricted to cases in which the boundary layer is fully turbulent over most of the wave cycle. On the basis of the measurements of *Jensen et al.* [1989], the onset of turbulence occurs within the first quarter of each half wave cycle ($\theta<45°$) for cases with $Re_o>1\times10^6$. For these cases the model is valid over most of the wave cycle. The data and model results suggest that the model can be used to describe velocity profiles and shear velocity at peak flow conditions ($u_o=u_{om}$) for $Re_o>5\times10^5$.

Time-Independent Versus Time-Dependent Eddy Viscosity

Time series of normalized mean (ensemble averaged) bottom shear stress, τ_0/τ_{0m}, over a half wave cycle measured by *Jensen et al.* [1989] using a hot film probe are shown by the symbols in Figure 5 for smooth turbulent flows ranging in Re_o from 1.6×10^6 to 6×10^6 (Jens 8, 9, 10; Table 1). The solid curves in Figure 5 give the temporal variation of normalized bottom shear stress computed using (5) and (6) and the time-independent, exponential form of K (K_E); computed and measured maximum shear velocities are given in Table 1. Near peak values, the measured and computed variation in boundary shear stress with phase agree reasonably well. At times of lower shear stress, however, there are marked differences between measured and computed boundary shear stress. During the accelerating part of the cycle, measured bottom shear stress exhibits a relatively abrupt change from lower, less variable mean bottom stresses to higher, more variable mean bottom stresses. The phase at which the shear stress makes this transition decreases with increasing Re_o. This suggests that even at Reynolds numbers as high as 6×10^6, the flow is not fully turbulent at the beginning of the accelerating phase. As discussed by *Jensen et al.* [1989] and *Hino et al.* [1983], the favorable pressure gradient during the accelerating phase inhibits turbulence production at small values of u_0. During deceleration, Figure 5 indicates that the measured bottom shear stress drops off somewhat more quickly than the values calculated with a time-independent eddy viscosity.

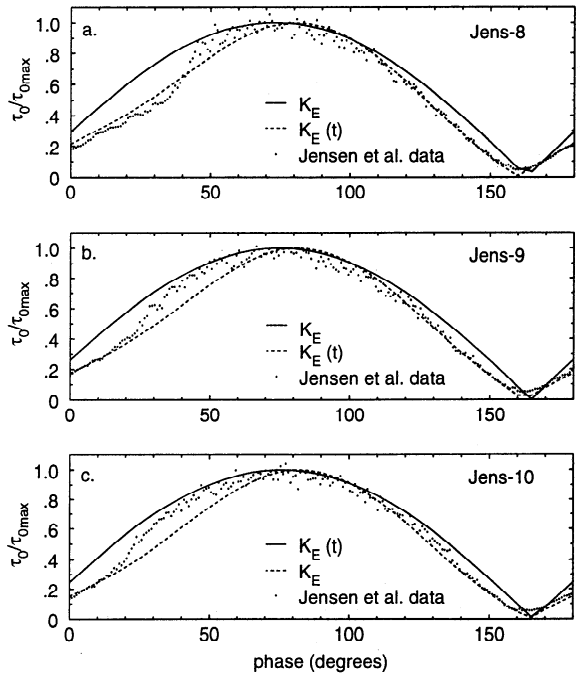

Figure 5. Boundary shear stress τ_0 normalized by the maximum bottom shear stress τ_{0max} as a function of phase over a half wave cycle for the smooth flow cases (a) Jens 8, (b) Jens 9, and (c) Jens 10 (Table 1) of *Jensen et al.* [1989]. The dots are the values of shear stress measured using a hot film sensor. The solid curves show the computed variation of τ_0/τ_{0max} using the time-independent, exponential form of eddy viscosity K_E. The dashed curves show the computed variation of τ_0/τ_{0max} using the time-dependent eddy viscosity $K_E(t)$ (see (6)).

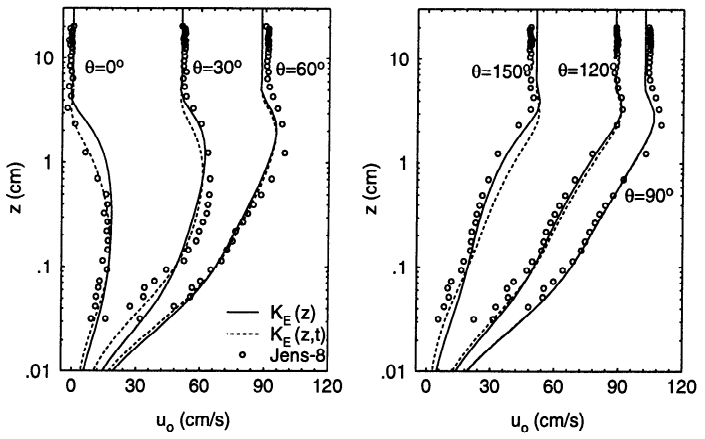

Figure 6. Comparison of velocity profiles for (left) accelerating and (right) maximum and decelerating phases computed using a time-dependent and time-independent form of the exponential eddy viscosity K_E for the smooth flow case Jens 8 of *Jensen et al.* [1989]. The open circles are the measured values, the solid line profiles are computed from (5) with steady form of K_E, and the dashed line profiles are computed with a time-dependent K_E.

Changes in hydraulic characteristics of the boundary layer over a wave cycle cannot be captured with a time-independent eddy viscosity because the velocity profile structure is set by the hydraulic conditions at maximum orbital velocity. This characterization optimizes the model for times of large shear stress, consistent with many of the applications of these models, but could be expected to overestimate turbulent mixing at times when the instantaneous shear stress is a minimum. To investigate the effects of time-independent versus time-varying formulations for eddy viscosity, the eddy viscosity given in (6) was modified, following the approach used by *Trowbridge and Madsen* [1984] for a rough turbulent wave boundary layer.

Trowbridge and Madsen [1984] suggest that the time-dependent variation of the turbulent eddy viscosity can be approximated using a truncated Fourier series, resulting in

$$K(z,t)=K_0(z)\,[\alpha(1+0.4\cos 2\,\omega t)] \qquad (11)$$

[*Trowbridge and Madsen*, 1984], retaining only the first two terms of the series. $K_0(z)$ is the time-independent eddy viscosity; the bracketed term effectively modifies the shear velocity in K_0 to produce a time-dependent turbulent velocity scale. The value of the constant α in (11) depends on the form of the turbulent velocity scale u_* used in (11). *Trowbridge and Madsen* [1984] use a two-part form of K_0 with average shear velocity, $\bar{u}_*$, as the velocity scale, in which case α=0.763. The velocity scale for K_0 used in the calculations presented herein is u_{*m}. In this case, α is adjusted to 0.714 so that the maximum value of the bracketed term is 1 and the instantaneous value of u_* cannot exceed u_{*m}.

Computed time series of bottom shear stress using the time-dependent eddy viscosity described above are indicated by the dashed curves in Figure 5 for the smooth turbulent flow cases, Jens 8, 9, and 10 (Table 1); in these calculations the bottom roughness is also time-varying, computed from the instantaneous shear velocity. Use of a time-dependent K accounts for more of the observed variation than does the time-independent form. At small values of instantaneous shear stress the calculations yield a variation of τ with time similar to that for a laminar flow because z^+ in (6) is small and hence K approaches ν through most of

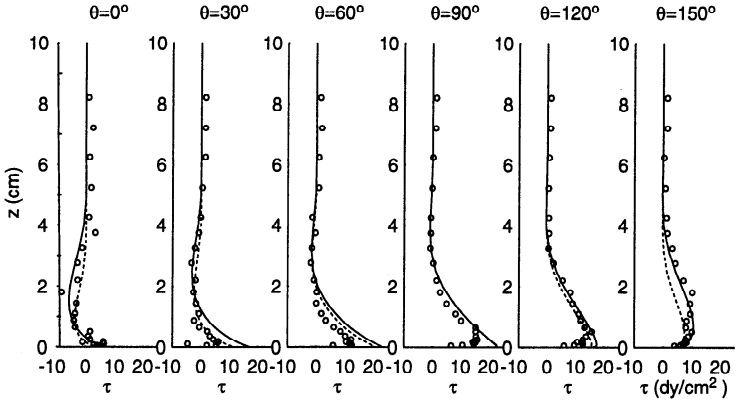

Figure 7. Comparison of computed shear stress profiles using time-dependent and time-independent forms of K_E for the smooth flow test Jens 8 (Table 1) of *Jensen et al.* [1989]. The open circles are measured values, the solid line profiles are computed using a steady form of K_E, and the dashed line profiles are computed using a time-varying form of K_E.

the boundary layer. However, the model does not attempt to represent the dynamics of the transition from laminar to turbulent flow and thus cannot predict the relatively abrupt increase in bottom shear stress observed in the data when the transition occurs during the accelerating phases. The model with a time-dependent eddy viscosity does a better job at representing the observed decrease of τ with time during the decelerating stage and is probably more reflective of the real processes controlling the variation of τ_0 with time at these phases.

Profiles of velocity and shear stress computed using time-dependent and time-independent forms of K_E (exponential form) are shown for case Jens 8 in Figures 6 and 7, respectively. In Figure 6, velocity profiles for accelerating and decelerating portions of a half wave cycle are shown. The time-varying K provides a better representation of the velocity profile at $u_o=0$ ($\theta=0$). It also more closely follows the measured velocity profiles near the bed at all phases. However, the time-independent form follows the data more closely in the outer part of the boundary layer, except at $\theta=0$. The flow is fully turbulent for $\theta>45°$, but residual turbulence is present in the boundary layer at all phases [*Jensen et al.*, 1989]. In Figure 7 the computed shear stress profiles are compared to measured Reynolds stress profiles at the same six phases of accelerating and decelerating flow; the computed stresses are the sum of the Reynolds and viscous stresses and thus do not follow the measured Reynolds stresses at the wall. The agreement in the near-wall region is somewhat better when the time-dependent eddy viscosity is used, but the agreement in the outer boundary layer is as good or better for the time-independent K.

Velocity and shear stress profiles at $u_o=0$ and $u_o=u_{om}$ computed with the time-dependent eddy viscosity for *Jonsson's* [1963] rough flow measurements and the *Jensen et al. [1989]* transitionally rough flow case, Jens 12, are shown in Figures 2 and 4, respectively. Profiles computed with a time-independent K agree at least as well with the measurements in both cases as those computed with a time-varying K. Examination of the full set of velocity profiles for the transitionally rough cases of *Jensen et al.* [1989] (Jens 12 and 13, Table 1) indicates a tendency, particularly at low orbital velocities, for the profiles to follow the time-dependent calculations in the lowest centimeter or so of the boundary layer and the time-independent calculations in the rest of the boundary layer. This is consistent with the strong local effects and small response time of turbulence near a wall compared to the outer regions of a boundary layer. In all cases the differences between profiles of velocity and shear stress computed with time-independent and time-varying forms of K become negligible at phases when orbital velocity is near its maximum value.

These results suggest that if detail at all phases is important, particularly for near-bed velocity and shear stress, employing a time-dependent eddy viscosity may be advisable. Accurate calculations of velocity and shear stress at initial accelerating phases for smooth turbulent flows require a more complex model that can account for the onset of turbulence under reversing pressure gradients [e.g., *Spalart and Baldwin*, 1989]. However, if one is primarily interested in the shear stress and velocity distribution at maximum velocity, then the additional effort involved in carrying out computations with a time-dependent form is probably not warranted, particularly given the degree of uncertainty that usually accompanies estimates of other parameters in the problem, especially bottom roughness.

Comparison of Measured and Computed Maximum Bottom Shear Stress

Solutions to the nondimensional form of the boundary layer equation for oscillatory flow (8) provide values for the ratio of maximum shear velocity to maximum orbital velocity u_{*m}/u_{om} as a function of the independent nondimensional parameters ξ_0 and Re_*. Because the maximum value of bed shear stress or shear velocity u_{*m} is not simultaneous with maximum orbital velocity at the top of the wave boundary layer u_{om}, the phase difference ϕ between these must be taken into account when computing u_{*m}/u_{om}. The resulting relationship is similar to *Jonsson's* [1966] wave friction factor diagram but is expressed in terms of the intrinsic nondimensional parameters of the governing equation, i.e., maximum shear velocity and the bottom roughness parameter z_0 rather than maximum orbital velocity and the physical bed roughness length k_s. The latter distinction is unimportant for hydraulically rough flow but is of consequence for smooth and transitionally rough flows in which z_0 also depends on viscous sublayer thickness. The relationships between shear velocity and orbital velocity derived herein are complementary to Jonsson's wave friction factor diagram and can be particularly useful for calculations in which bottom shear stress or shear velocity rather than orbital velocity is known, as in threshold sediment transport calculations.

Wave friction factor f_w is defined by $f_w=2(u_{*m}/u_{om})^2$ and typically is expressed as a function of the ratio of wave orbital amplitude to physical bottom roughness length (a_o/k_s) and wave Reynolds number $Re_o=u_{om}a_o/\nu$. These are related to the parameters ξ_0 and Re_* as follows:

$$\frac{a_o}{k_s}=\frac{u_{om}}{\omega k_s}=\frac{1}{\xi_0}\frac{u_{om}}{u_{*m}}\frac{z_0}{k_s} \tag{12a}$$

$$Re_o=\frac{u_{om}^2\omega}{\nu}=Re_*\left[\frac{u_{om}}{u_{*m}}\right]^2 \tag{12b}$$

Thus values of ξ_0 and Re_* can be transformed to equivalent values of a_o/k_s and Re_o, given u_{*m}/u_{om} and z_0/k_s; the latter is a function of roughness Reynolds number $R_*=u_*k_s/\nu$ [e.g., *Smith*, 1977]. The product $\xi_0 Re_*$ is equal to the product R_*z_0/k_s. For any value of the product $\xi_0 Re_*$, only one value of R_* with its accompanying value of z_0/k_s will satisfy this equality, except for smooth turbulent flows, in which case $\xi_0 Re_*$ is always equal to 0.11, so that R_* and z_0/k_s cannot be uniquely determined. The unsteady boundary layer equations cannot be posed directly in terms of the independent variable u_o and k_s because eddy viscosity depends on u_* as does z_0 for smooth and transitionally rough flows.

For comparison with previous work, asymptotic relationships between u_{*m}/u_{om}, ξ_0, and Re_* computed using the nondimensional boundary layer equation (8) for smooth and rough turbulent flow conditions have been converted into curves of f_w as a function of Re_o and a_o/k_s, respectively, using (12a) and (12b). The results for smooth turbulent

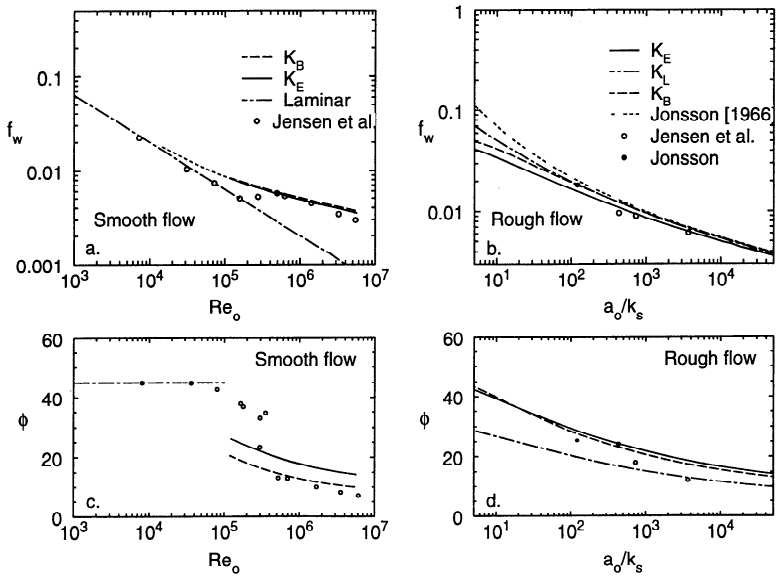

Figure 8. Comparison of computed and measured maximum boundary shear stress for smooth and rough turbulent flow. (a) Wave friction factor $f_w=2(u_{*m}/u_{om})^2$ as a function of $Re_o=u_o^2/(\omega\nu)$ for smooth wave boundary layer flow. Computed curves are shown for exponential K_E and two-part K_B eddy viscosities; the theoretical relationship for a laminar oscillatory boundary layer is also given. Measured values for laminar and smooth turbulent cases (Jens 1-10, Table 1) from *Jensen et al.* [1989] are shown for comparison. (b) Wave friction factor as a function of a_o/k_s for rough oscillatory flow. Computed curves are shown for a linear eddy viscosity K_L in addition to the two forms of K shown in Figure 10a. Measured rough flow values from *Jensen et al.* [1989] (Jens 13-15, Table 1) and *Jonsson* [1963] and *Jonsson*'s [1966] semiempirical friction factor curve for rough flow are indicated for comparison. (c) Phase difference ϕ between $u(z)$ and u_{om}, in degrees, for smooth turbulent flow. (d) Same as Figure 8c, but for rough turbulent flow.

flow are shown in Figures 8a and 8c. The symbols indicate the laminar, transitionally turbulent, and smooth turbulent flow measurements of *Jensen et al.* [1989], Jens 1 through 10 in Table 1. For comparison, computed curves of f_w as a function of the Reynolds number Re_o are plotted for the exponential K_E and two-part K_B forms of eddy viscosity; the difference between the curves for these two eddy viscosities is negligible. The analytical solution for a laminar oscillatory boundary layer is also shown. The data show that wave boundary layer flow at peak velocity ($u_o=u_{om}$) is turbulent for $Re_o>5\times10^5$. The agreement between the measured and computed friction factors is generally good for the smooth turbulent cases, although both computed curves appear to overpredict the measured bottom shear stresses at the highest values of Re_o. The average discrepancy in f_w for the smooth turbulent cases is 0.008 for K_E and 0.011 for K_B. The results for the phase difference between maximum bottom shear stress and maximum orbital velocity are similar. The phase difference changes markedly as the boundary layer becomes turbulent, with ϕ dropping to about 10°. Here the two-part eddy viscosity better reproduces the measured phase lags for the smooth turbulent cases than does the exponential form. Phase lags for the exponential eddy viscosity are smaller when the time-varying form $K_E(t)$ is used, averaging about 10° for the smooth and rough turbulent flow cases.

The results for rough flow conditions are shown in Figures 8b and 8d. The symbols indicate the rough turbulent flow measurements of *Jensen et al.* [1989] and *Jonsson* [1963], cases Jens 13 through 15 and Jons 1 in Table 1. For comparison, computed curves of friction factor as a function of a_o/k_s are plotted for the exponential K_E, linear K_L, and two-part K_B forms of eddy viscosity. *Jonsson*'s [1966] approximate expression for wave friction factor under rough flow conditions, $(4\sqrt{f_w})^{-1} + \log(4\sqrt{f_w})^{-1} = -0.08+\log(a_o/k_s)$ is also shown. The *Jensen et al.* [1989] data appear to be best represented by the K_E curve, whereas the *Jonsson* [1963] value is more closely predicted by either K_L or K_B. The average discrepancy in f_w is 0.008 for K_E, 0.013 for K_L, and 0.013 for K_B. The differences between these computed curves are relatively minor for values of $a_o/k_s>100$. The computed curves and *Jonsson*'s [1963] approximate expression deviate more at lower values of a_o/k_s. However, both the present analysis and *Jonsson*'s [1963, 1966] analyses indicate that the computed values of f_w are questionable at values of $a_o/k_s<10$ because assumptions regarding separation of length scales in the formulation of (5) are violated. The computed phase differences for the rough flow cases are similar for K_E and K_B and are somewhat lower for K_L. The data fall between the two computed trends.

In converting from z_0 to k_s, it has been assumed that bed roughness can be expressed in terms of equivalent bed roughness so that, for example, $k_s=30z_0$ for rough flow, following *Nikuradse* [1933]. For planar beds of relatively well-sorted sediment, this is reasonable, and in this case the shear stress related to u_{*m} or f_w is the shear stress acting on the bed, e.g., the shear stress available to transport sediment. The problem is more difficult when ripples or other larger-scale roughness elements are present on the bed as is often the case under waves.

Two problems arise when applying this analysis to rippled beds. The first has to do with the proper parameterization of ripple roughness and the relationship between z_0 and

k_s. A reasonable estimate of z_0 for wave-generated ripples is provided by $(z_0)_{ripples}=\eta^2/\lambda$, where η is ripple height and λ is ripple length [*Grant and Madsen*, 1982; *Wiberg and Nelson*, 1992]. When ripple roughness is large, the magnitude of z_0 can approach the value of δ_w and ripple height can exceed δ_w, although this occurs more commonly in laboratory flumes than on the continental shelf [*Wiberg and Harris*, 1994]. As noted previously, wave boundary layer height must be significantly larger than z_0 for the theory presented here to apply. The other difficulty is that the shear stress given by f_w or u_{*m}/u_{om} is not the shear stress acting on the bed surface when the dominant roughness scale is the ripple roughness. Some correction for bed form drag [e.g. *Einstein*, 1950; *Smith and McLean*, 1977] must be included in the calculations when relating bed shear stress (skin friction) to the boundary shear stress computed using a ripple roughness for k_s [see *Wiberg and Nelson*, 1992].

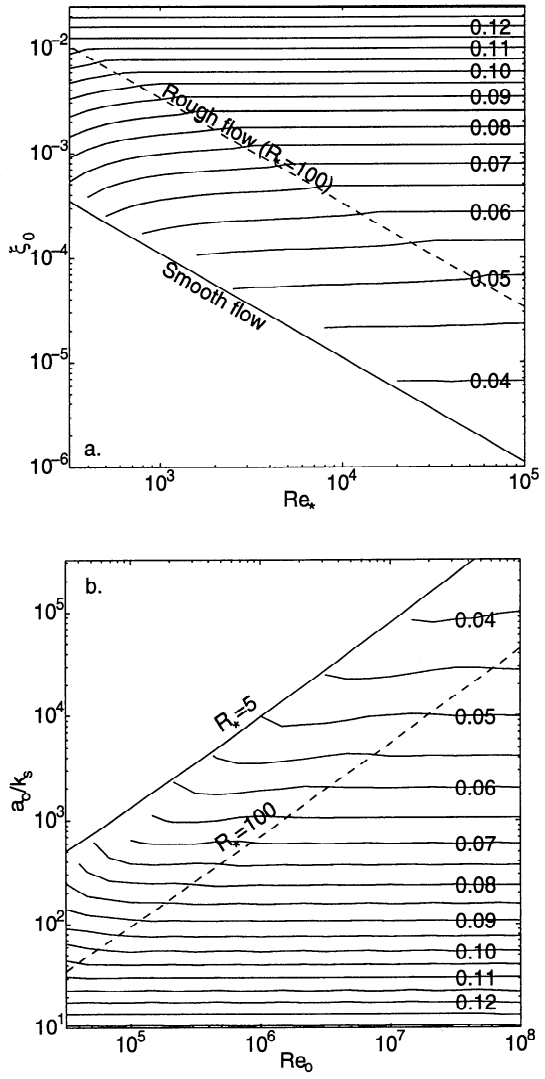

Figure 9. (a) Contour plot of u_{*m}/u_{om} as a function of ξ_0 and Re_*. Curves for smooth turbulent flow and the approximate lower bound of fully rough turbulent flow (R_*=100) are indicated. (b) Contour plot of u_{*m}/u_{om} as a function of Re_o and a_o/k_s. Curves for R_* of 5 and 100 are given, corresponding approximately to the upper and lower bounds of smooth and fully rough turbulent flow, respectively. The contour interval in both plots is 0.005.

The relationship between u_{*m}/u_{om}, ξ_0, and Re$_*$ computed using (8) over the full parameter range, including transitionally rough flow, defines a surface. A contour plot of the surface, giving u_{*m}/u_{om} as a function of Re_* and ξ_0 is shown in Figure 9a. Numbers near the right ends of the contours give the values of u_{*m}/u_{om} for alternate contours; the contour interval is 0.005. Re_* values of roughly 1000 or less correspond to flows in which laminar or transitionally turbulent conditions, which the model cannot accurately represent, extend to peak flow phases. Curves of equal roughness Reynolds number R_* form a set of parallel lines on this plot. Lines indicating smooth turbulent flow conditions and R_*=100, approximately the lower bound of fully rough turbulent flow, are indicated on Figure 9. In the fully rough turbulent flow region, above $R_*\approx$100, the contours of u_{*m}/u_{om} are horizontal lines independent of Re_*.

The corresponding contour plot of u_{*m}/u_{om} in terms of the alternate parameter set, Re_o and a_o/k_s, is given in Figure 9b. In this case, values of Re_o of roughly 5×10^5 and less correspond to cases in which transitionally turbulent conditions extend to peak flow phases. Curves of R_* equal to 5 and 100, approximately the upper and lower bounds for fully smooth and rough turbulent flow, respectively, are indicated on the plot. The contours in Figure 9b are similar to those in Figure 9a but have a somewhat more variable structure owing to the form of the z_0/k_s relationship with R_*, which enters into the transformation from ξ_0 to a_o/k_s.

Values of u_{*m}/u_{om} can also be presented in two-dimensional plots of u_{*m}/u_{om} as a function of ξ_0 at constant values of Re_* (Figure 10a) and as a function of Re_* at constant values of ξ_0 (Figure 10b). The latter is comparable to *Jonsson*'s [1966] friction factor diagram. Given wave period, fluid viscosity, the bottom roughness parameter, and maximum shear velocity, these plots can be used to determine the corresponding value of maximum near-bed wave orbital velocity. Note that u_{*m}/u_{om} varies slowly compared to Re_* and ξ_0, except under laminar flow conditions. For values of $Re_*\geq$5000, curves of u_{*m}/u_{om} versus ξ_0 nearly lie on top of each other in Figure 10a, defining the rough flow relationship which, as noted previously, is independent of Re_*. At lower values of Re_*, only a portion of the curves in Figure 10a follow the rough flow limit, consistent with the conditions for rough flow noted in a previous section. Rough flow is seen in Figure 10b as the region in which the curves parallel the Re_* axis. Smooth flow in both figures is indicated by a dotted curve. The stippled region of Figure 10b indicates the general range of conditions in which the boundary layer would be expected to be laminar or transitionally turbulent. The theoretical laminar flow relationship, $u_{*m}/u_{om}=(2\,Re_*)^{-1}$, is indicated by the dashed curve in Figure 10b. Between the smooth flow curve and the R_*=100 curve is the region of transitionally rough turbulent flow.

Conclusions

Solutions to the unsteady boundary layer equation (5) give profiles of velocity and shear stress in the wave boundary layer through a wave cycle. The eddy viscosity formulation used in this analysis, which employs *Reichardt*'s [1951] interpolating profile for the region of flow between the viscous sublayer and the overlying logarithmic flow layer, allows velocity and shear stress to be computed for

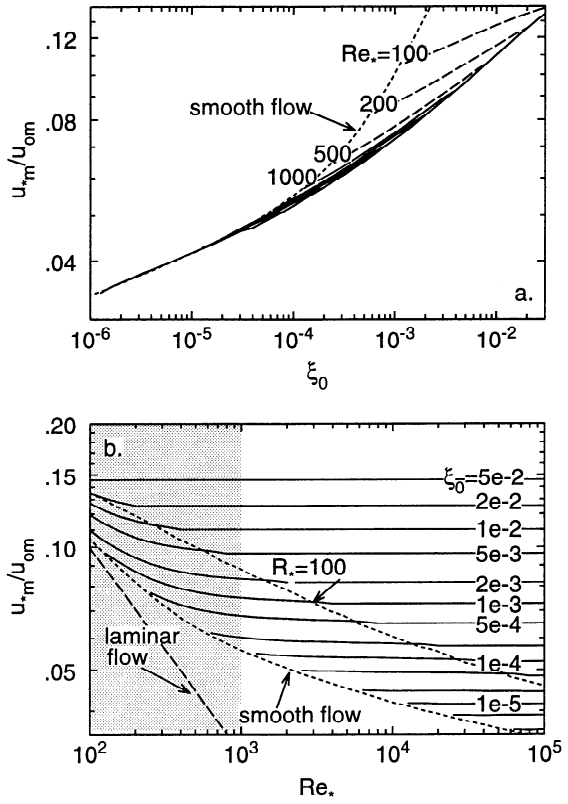

Figure 10. Curves of (a) u_{*m}/u_{om} as a function of ξ_0 for the constant values of Re_* as indicated (b) u_{*m}/u_{om} as a function of Re_* for the constant values of ξ_0 indicated. Curves indicating the transitions to rough and smooth turbulent flow are given; the stippled region in Figure 10b provides a general indication of transitionally turbulent conditions for which the model does not apply.

any roughness Reynolds number, including smooth and transitionally rough flows. Comparison between calculated and measured velocity and shear stress profiles for the *Jonsson* [1963] and *Jensen et al.* [1989] oscillatory boundary layer experiments indicate that both the exponential and two-part forms of eddy viscosity considered herein provide a reasonable characterization of turbulent mixing in an oscillatory boundary layer; the agreement is significantly poorer for a linear eddy viscosity. Use of a time-independent eddy viscosity, with maximum shear velocity as the velocity scale, yields profiles of velocity in good agreement with measured smooth, transitionally rough, and rough flow profiles at maximum velocity and generally throughout a wave period, particularly in the outer part of the boundary layer. Profiles of velocity and shear stress computed using a time-varying eddy viscosity generally give better agreement with measured values near the bed. Maximum boundary shear stress is well predicted with either a time-independent or time-varying form of eddy viscosity.

Computed ratios of maximum shear velocity to maximum orbital velocity compare favorably with available smooth and rough flow measurements from *Jonsson* [1963] and *Jensen et al.* [1989] and *Jonsson*'s [1966] wave friction factor relationship for rough flow. The calculated relationship between maximum shear velocity and maximum orbital velocity in an oscillatory boundary layer is a function of two nondimensional variables. The two independent variables can be expressed in terms of "outer" flow parameters, u_{om} and k_s, or "inner" flow parameters, u_{*m} and z_0. The dimensionless variables $\xi_0=z_0\omega/u_{*m}$ and $Re_*=u_{*m}\delta_w/\nu$ arise naturally when the unsteady boundary layer equation is nondimensionalized. Commonly used forms of the eddy viscosity can also be readily nondimensionalized in terms of these parameters. The inner flow parameters, ξ_0 and Re_*, can be related to the corresponding outer flow variables, a_o/k_s and $Re_o=u_{om}a_o/\nu$, which are often convenient and are commonly used but cannot be substituted directly into the governing equation. The parameters ξ_0 and Re_* are directly related to roughness Reynolds number so that criteria for smooth, transitionally rough, and rough flow can be readily defined (Figure 9).

Use of these results is relatively straightforward for moderately well-sorted, planar beds. Natural flows are commonly complicated by the presence of ripples on the bed. At best, this necessitates some consideration of bed form drag when estimating bed shear stress (skin friction). At worst, large values of bed form roughness relative to wave boundary layer thickness can create a situation in which the ripples are not fully submerged in the wave boundary layer and the assumptions underlying the unsteady boundary layer formulation employed herein are violated [*Wiberg and Harris*, 1994].

Acknowledgments. This work was supported by the Office of Naval Research STRESS program under grant N00014-91-J-1349. I would like to thank B. Jensen, B. Sumer, and J. Fredsøe for generously providing me with their oscillatory boundary layer measurements and John Trowbridge and several anonymous reviewers for helpful comments on earlier drafts of this paper.

References

Agrawal, Y.C., and D.G. Aubrey, Velocity observations above a rippled bed using laser Doppler velocimetry, *J. Geophys. Res., 97*, 20,249-20,259, 1992.

Brevik, I., Oscillatory rough turbulent boundary layers, *J. Waterw. Port Coastal Ocean Div. Am. Soc. Civil Eng., 107*, 175-188, 1981.

Businger, J.A., and S.P.S. Arya, Height of the mixed layer in the stably stratified planetary boundary layer, in *Advances in Geophysics*, pp. 73-92, Academic, San Diego, Calif., 1974.

Carnahan, B., H.A. Luther, and J.O. Wilkes, *Applied Numerical Methods*, John Wiley, New York, 1969.

Einstein, H.A., The bed-load function for sediment transport in open channel flows, *Tech. Bull. 1026,* pp. 1-71, U.S. Dep. of Agric. Soil Conserv. Serv., Washington, D.C., 1950.

Fredsøe, J., Turbulent boundary layer in wave-current motion, *J. Hydraul. Eng., 110*, 1103-1120, 1984.

Grant, W.D., and O.S. Madsen, Combined wave and current interaction with a rough bottom, *J. Geophys. Res., 84*, 1797-1808, 1979.

Grant, W.D., and O.S. Madsen, Movable bed roughness in unsteady oscillatory flow, *J. Geophys. Res., 87*, 469-481, 1982.

Hino, M., M. Kashiwayanagi, A. Nakayama, and T. Hara, Experiments on the turbulence statistics and the structure of a reciprocating oscillatory flow, *J. Fluid Mech., 131*, 363-400, 1983.

Jensen, B.L., Experimental investigation of turbulent oscillatory boundary layers, *Ser. Pap. 45*, 157 pp., Inst. of Hydrodyn. and Hydraul. Eng., Tech. Univ. of Denmark, Lyngby, 1989.

Jensen, B.L., B.M. Sumer, and J. Fredsøe, Turbulent oscillatory boundary layers at high Reynolds numbers, *J. Fluid Mech., 206*, 265-297, 1989.

Jonsson, I.G., Measurements in the turbulent wave boundary layer, paper presented at 10th Congress, Int. Assoc. of Hydraul. Res., London, 1963.

Jonsson, I.G., Wave boundary layers and friction factors, paper presented at 10th Coastal Engineering Conference, Am. Soc. of Civil Eng., Tokyo, September 1966.

Jonsson, I.G., and N.A. Carlsen, Experimental and theoretical investigations in an oscillatory turbulent boundary layer, *J. Hydraul. Res., 14*, 45-60, 1976.

Kajiura, K., A model of the bottom boundary layer in water waves, *Bull. Earthquake Res. Inst. Univ. Tokyo, 46*, 75-123, 1968.

Kamphuis, J.W., Friction factor under oscillatory waves, *J. Waterw. Port Coast. Ocean Div. Am. Soc. Civil Eng., 101*, 135-144, 1975.

Long, C.E., A simple model for time-dependent, stably stratified turbulent boundary layers, Ph.D. thesis, 170 pp., Univ. of Wash., Seattle, 1981.

Madsen, O.S., Wave climate of the continental margin: Elements of its mathematical description, in *Marine Sediment Transport and Environmental Management*, edited by D.J. Stanley and D.J.P. Swift, pp. 65-87, Wiley-Intersci., New York, 1976.

Myrhaug, D., On a theoretical model of rough turbulent wave boundary layers, *Ocean Eng., 9*, 547-565, 1982.

Nezu, I., and W. Rodi, Open-channel flow measurements with a laser Doppler anemometer, *J. Hydraul. Eng., 112*, 335-355, 1986.

Nikuradse, J., Laws of flow in smooth pipes, *NASA Tech. Transl., F10359* (1966), 74 pp., Washington, D.C., 1932.

Nikuradse, J., Laws of flow in rough pipes (translation), *Tech. Memo. 1292* (1950), Natl. Advisory Comm. for Aeronaut., Washington, D.C., 1933.

Reichardt, H., Vollstandige Darstellung der turbulenten Geschwindigkeitsverteilung in glatten Leitungen, *Z. Angew. Math. Mech., 31*, 1951.

Schlichting, H., *Boundary Layer Theory*, 7th ed., 817 pp., McGraw-Hill, New York, 1979.

Sleath, J.F.A., Turbulent oscillatory flow over rough beds, *J. Fluid Mech., 182*, 369-409, 1987.

Smith, J.D., Modeling of sediment transport in continental shelves, in *The Sea*, vol. 6, edited by E.D. Goldberg, pp. 539-577, Wiley-Intersci., New York, 1977.

Smith, J.D., and S.R. McLean, Spatially averaged flow over a wavy surface, *J. Geophys. Res., 82*, 1735-1746, 1977.

Spalart, P.R., and B.S. Baldwin, Direct simulation of a turbulent oscillating boundary layer, in *Turbulent Shear Flows*, vol. 6, edited by J.-C. Andre et al., pp. 417-440, Springer-Verlag, New York, 1989.

Trowbridge, J., and O.S. Madsen, Turbulent wave boundary layers, 1, Model formulation and first-order theory, *J. Geophys. Res., 89*, 7989-7997, 1984.

van Driest, E.R., On turbulent flow near a wall, *J. Aeronaut. Sci., 23*, 1007-1011, 1956.

Wiberg, P.L., and C.K. Harris, Ripple geometry in wave-dominated environments, *J. Geophys. Res., 99*, 775-789, 1994.

Wiberg, P.L., and J.M. Nelson, Unidirectional flow over asymmetric and symmetric ripples, *J. Geophys. Res., 97*, 12,745-12,761, 1992.

Wiberg, P.L., and J.D. Smith, Calculations of the critical shear stress for motion of uniform and heterogeneous sediments, *Water Resour. Res., 23*, 1471-1480, 1987.

P. L. Wiberg, Department of Environmental Sciences, University of Virginia, Charlottesville, VA 22903 (e-mail: pw3c@virginia.edu).

(Received April 29, 1993; revised July 27, 1995; accepted August 2, 1995.)